An evaluation on mechanisms of miscibility development in acid gas injection for volatile oil reservoirs

Erhui Luo, Zifei Fan, Yongle Hu, Lun Zhao, Jianjun Wang

Oil & Gas Science and Technology - Rev. IFP Energies nouvelles **74**, 59 (2019)

https://doi.org/10.2516/ogst/2019018

Available online at:
ogst.ifpenergiesnouvelles.fr

REGULAR ARTICLE OPEN ACCESS

An evaluation on mechanisms of miscibility development in acid gas injection for volatile oil reservoirs

Erhui Luo*, Zifei Fan, Yongle Hu, Lun Zhao, and Jianjun Wang

PetroChina Research Institute of Petroleum Exploration & Development, Beijing 100083, China

Received: 25 December 2018 / Accepted: 20 March 2019

Abstract. Produced gas containing the acid gas reinjection is one of the effective enhanced oil recovery methods, not only saving costs of disposing acid gases and zero discharge of greenhouse gases but also supporting reservoir pressure. The subsurface fluid from the Carboniferous carbonate reservoir in the southern margin of the Pre-Caspian basin in Central Asia has low density, low viscosity, high concentrations of H_2S (15%) and CO_2 (4%), high solution gas/oil ratio. The reservoir is lack of fresh water because of being far away onshore. Pilot test has already been implemented for the acid gas reinjection. Firstly, in our work a scheme of crude oil composition grouping with 15 compositions was presented on the basis of bottomhole sampling from DSTs of four wells. After matching PVT physical experiments including viscosity, density and gas/oil ratio and pressure–temperature (P–T) phase diagram by tuning critical properties of highly uncertain heavy components, the compositional model with phase behavior was built under meeting accuracy of phase fitting, which was used to evaluate mechanism of miscibility development in the acid gas injection process. Then using a cell-to-cell simulation method, vaporizing and/or condensing gas drive mechanisms were investigated for mixtures consisting of various proportions of CH_4, CO_2 and H_2S in the gas injection process. Moreover, effects of gas compositions on miscible mechanisms have also been determined. With the aid of pressure-composition diagrams and pseudoternary diagrams generated from the Equation of State (EoS), pressures of First Contact Miscibility (FCM) and Multiple Contact Miscibility (MCM) for various gases mixing with the reservoir oil sample under reservoir temperature were calculated. Simulation results show that pressures of FCM are higher than those of MCM, and CO_2 and H_2S are able to reduce the miscible pressure. At the same time, H_2S is stronger. As the CH_4 content increases, both pressures of FCM and MCM are higher. But incremental values of MCM decrease. In addition, calculated envelopes of pseudoternary diagrams for mixtures of CH_4, CO_2 and H_2S gases of varying composition with acid gas injection have features of bell shape, hourglass shape and triangle shape, which can be used to identify vaporizing and/or condensing gas drives. Finally, comparison of the real produced gas and the one deprived of its C_3^+ was performed to determine types of miscibility and calculate pressures of FCM and MCM. This study provides a theoretical guideline for selection of injection gas to improve miscibility and oil recovery.

1 Introduction

Gas injection is an important enhanced oil recovery process, in which interphase mass transfer during multiple contacting of the injected gas and the reservoir oil results in an efficient displacement. Reinjection into the reservoir of a gas produced from an oil field is commonly used. While the reasons are lack of transport pipelines and saving cost of disposing produced gas, much interest is being devoted to gas injection as an enhanced oil recovery process. Obviously, reinjection of the gas reduces the pressure drop associated with production of oil from a field. Moreover, immiscible/miscible gas injection can occur when the injected gas diffuses into the oil, and the oil will swell and oil viscosity reduces. If the interfacial tension is eliminated, miscible gas drive occurs. However, the injected gas also affects the oil/gas equilibrium compositions in the reservoir. Injection of various gases involving CO_2 and acid gas into the oil reservoir has been investigated by some authors. There is the miscible HC gas reinjection project with large volumes of sour gas (3–4% H_2S and 10–15% CO_2) at Harweel field in Oman (Al-Hadhrami *et al.*, 2007). The pilot project is a first contact miscible gas injection with 12% H_2S content which has recently been running in the Tengiz oilfield in Kazakhstan (Wang *et al.*, 2014; Urazgaliyeva *et al.*, 2014). CO_2 injection has also made a good progress (Luo *et al.*, 2013a, b).

Miscibility development has two different processes: First Contact Miscibility (FCM) and Multiple Contact

* Corresponding author: luoerhui2006@163.com

Miscibility (MCM). If a single phase is formed when the original oil and the injected gas become fully miscible, the oil and gas phases exhibit FCM. If the original oil and the injected gas need multiple contacts to achieve miscibility, MCM will happen. The traditional interpretation of the MCM indicates that the gas may take up components from the oil phase corresponding to the vaporizing gas drive, the oil may take up components from the gas phase corresponding to the condensing gas drive. Later, a combined vaporizing/condensing mechanism was presented to describe MCM (Zick, 1986; Stalkup, 1987; Johns *et al.*, 2002). Multiple contact experiments were conducted to study the effect of phase behavior on CO_2 flood (Gardner *et al.*, 1981). Abrishami and Hatamian (1996) studied the thermodynamic behavior of hydrocarbon fluids in multiple contact processes with non-hydrocarbon (N_2, CO_2 and their mixtures) through experiments. Ternary diagrams are commonly used to decide whether or not miscibility has been achieved. A cell-to-cell simulation program was presented by Metcalfe *et al.* (1973). Pederson *et al.* (1986) used a cell-to-cell model in connection with a ternary diagram to simulate a miscible drive. Nutakki *et al.* (1991) interpreted the mechanism of oil recovery as a condensing/vaporizing process with significant upper phase extraction on the basis of pseudoternary diagrams and pressure-composition diagrams generated from the Equation of State (EoS). Tang *et al.* (2005) evaluated the miscible ability and mechanism of gas displacement by simulating the PVT experiment data, pressure-composition experiment, multiple contact miscible experiment and slim-tube experiment available. Johns *et al.* (2010) calculated Minimum Miscibility Pressure (MMP) for oils displaced by CO_2 contaminated by mixtures of N_2, CH_4, C_2, C_3, and H_2S. Belhaj *et al.* (2013) evaluated miscible oil recovery utilizing N_2 and/or HC gases in CO_2 injection. It is clear that the major research focuses on CO_2 injection or CO_2 mixtures with other gases, but there are very limited studies on acid gas injection with high H_2S content (Zhang *et al.*, 2017; Luo *et al.*, 2018).

In this paper, a simulation study was conducted to evaluate the performance of the acid gas miscible injection process. Pseudoternary diagrams are used to represent the mixing processes which take place in a petroleum reservoir into which gas is being injected. Mixtures consisting of various proportions of reservoir oil and injection gas (static mixtures of 0 mol%–90 mol% injection gas) were calculated to generate the pressure-composition diagram for the multicomponent system. Multiple-contact calculations were then performed at a pressure equal to the flooding pressure and the pseudoternary diagram was generated. The principal mechanisms of the oil recovery were then identified using the many-component pressure-composition diagram and pseudoternary diagram.

2 Phase behavior modeling and PVT matching

2.1 Phase behavior modeling

In order to access the acid gas flooding, the oil samples utilized are from the Carboniferous carbonate reservoir located in the southern part of the Pri-Caspian basin marginal zone. There are four wells (well X-1, well X-2, well X-3 and well X-6) that have been performed six DSTs to obtain representative bottomhole fluids samples. To make sure the good quality of the sampled fluids, the flowing bottomhole pressure during sampling is larger than the saturation pressure. The routine PVT data includes Constant Mass Expansion (CCE) and Differential Liberation (DL) for the reservoir fluids. The saturation point of the reservoir fluid is found to be 28.4 MPa at 98 °C. Column 2 of Table 1 shows the composition of the reservoir oil sample. The acid gas component ($H_2S + CO_2$) mole fraction in the oil sample is 19.23%.

The solution Gas-Oil Ratio (GOR) is high (640–670 m^3/m^3). The produced fluid was separated by the three-stage separator (Fig. 1). The conditions of high pressure, middle pressure and low pressure separators are 9.6 MPa, 3.0 MPa, 8.5 MPa and 70 °C, 60 °C, 52 °C respectively. The produced gas is exported directly to shore except reinjection gas and fuel gas. Because every separator has different pressure and temperature, GOR and H_2S concentration of every separator is varied that leads to the compressor with various gas compositions. Column 3 of Table 1 shows the composition of the produced gas injected into the reservoir. To compare the effect of the gas composition, the produced gas is deprived C_3^+, named deprived C_3^+.

2.2 Laboratory PVT data matching

A detailed description of sample oils was obtained from experimental analysis. The oil was split into 14 components including 5 pseudocomponents for the heavy fraction. The Peng-Robinson Equation of State (EoS) was selected to predict thermodynamic properties. These component properties (critical pressure P_c, critical temperature T_c, and ancient factor ω) of heavy components were adjusted to match experimental data which include CCE and DL. The regression procedure of Agarwal *et al.* (1990) was used in the data matching. The oil viscosity, oil density and GOR calculated with 14 components are reported in Figures 2, 3 and 4 respectively showing good agreement with these experimental data. Figure 5 shows the discrepancies between post-match and pre-match of P–T phase diagrams. It is obvious that the P–T phase diagram after matching is enlarged and the saturation pressure at the reservoir temperature of 98 °C shows excellent agreement. A 14-component data set of thermodynamic properties was generated (Tab. 2). This is very useful in evaluating mechanisms of miscibility development of the acid gas injection.

3 Evaluation on mechanisms of vaporizing and condensing gas drive

Gas injection into a petroleum reservoir can be simulated using a cell-to-cell calculation presented by Metcalfe *et al.* (1973) and Pederson *et al.* (1986). This method simulates a number of cells of equal volumes in a series as shown in Figure 6. The temperature and the pressure are the same in each cell, and the volume is kept constant. Initially all

Table 1. Composition of oil and two types of injection gas.

Component	Crude oil	Produced gas	Deprived C_3^+
H_2S	0.151	0.15905	0.168
CO_2	0.0413	0.05463	0.058
N_2	0.00835	0.01164	0.013
C_1	0.4703	0.63579	0.669
C_2	0.073	0.08538	0.092
C_3	0.0415	0.03426	0
C_4	0.03052	0.01386	0
C_5	0.02061	0.00386	0
C_6	0.0165	0.00105	0
C_7–C_9	0.0538	0.00048	0
C_{10}–C_{15}	0.05532	0	0
C_{16}–C_{21}	0.02081	0	0
C_{22}–C_{27}	0.00882	0	0
C_{28}^+	0.00817	0	0

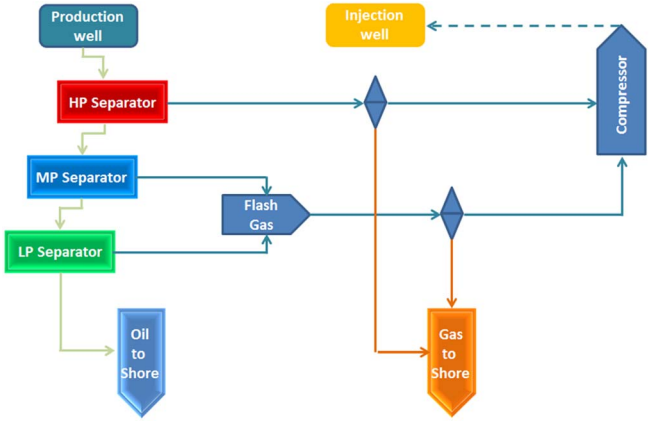

Fig. 1. Surface oil and gas separation process.

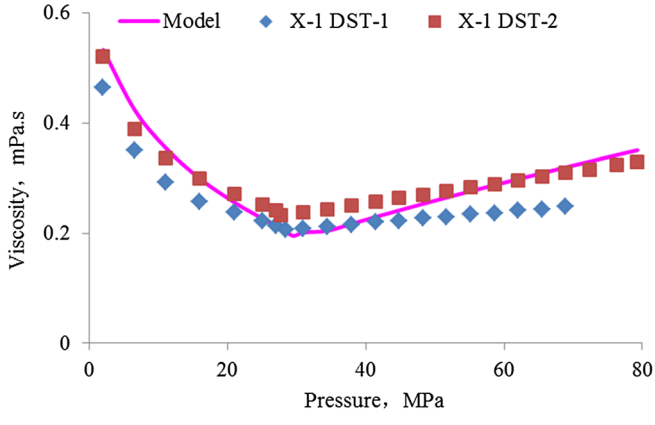

Fig. 2. Oil viscosity curves and their fitting.

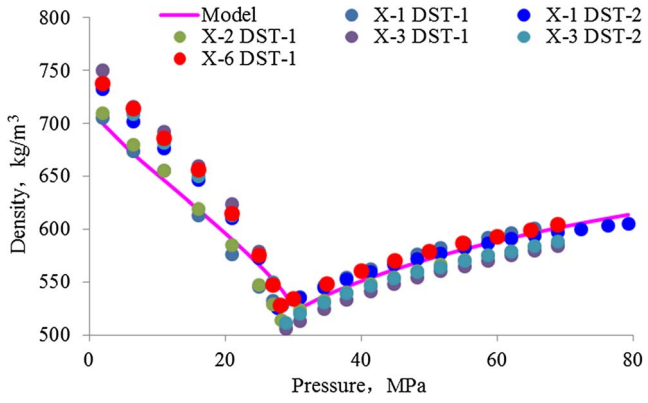

Fig. 3. Oil density curves and their fitting.

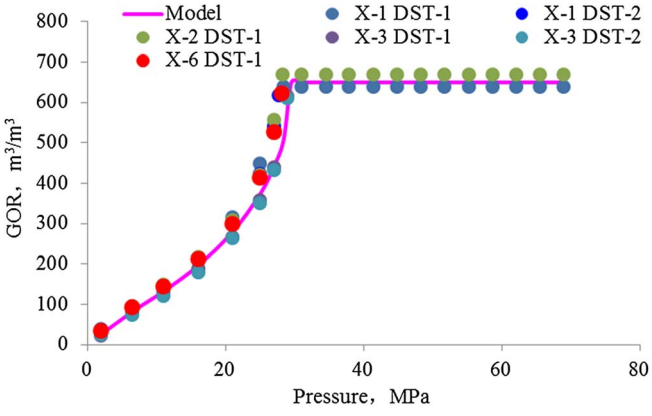

Fig. 4. GOR curves and their fitting.

the cells contain the same fluid compositions. A specified amount of gas is added to cell 1. A flash calculation is performed in each cell when mixing takes place and thermodynamic equilibrium is attained. After mixing of the injected gas and the cell fluid, the excess volume from cell 1 is transferred to cell 2. The excess volume from cell 2 is transferred to cell 3, etc.

Pseudoternary diagrams are commonly used to decide whether or not miscibility has been achieved. Based on 14 pseudocomponents of the petroleum mixture, the composition of this mixture is represented using three groups of components, C_1+N_2, C_2-C_5+CO_2+H_2S and C_6^+. In order to use a pseudoternary diagram in connection with a cell-to-cell method, the following steps are used to calculate the MMPs and generate pseudoternary diagrams for MCM processes at a given temperature:

1. Choose a range of pressures.
2. Gas is added to oil at specified gas to oil molar ratio increments and flash calculations are performed until two-phase region is detected.
3. Using the first point in the two-phase region detected in step 2, the flashed liquid is mixed with the original gas at the specified gas to liquid ratio and the flash

Table 2. Thermodynamic properties of the pseudocomponents.

Component	M_w (kg/mol)	T_c (K)	P_c (atm)	V_c (m^3/kg · mole)	Z_c	Boil (°C)	ω	Parachor
H_2S	34.1	373.2	88.20	0.099	0.284	−60.4	0.100	80.1
CO_2	44.0	304.2	72.80	0.094	0.274	−78.5	0.225	78.0
N_2	28.0	126.2	33.50	0.090	0.290	−195.8	0.040	41.0
C_1	16.0	190.6	45.40	0.099	0.287	−161.5	0.008	77.0
C_2	30.1	305.4	48.20	0.148	0.285	−88.7	0.098	108.0
C_3	44.1	369.8	41.90	0.203	0.280	−42.1	0.152	150.3
C_4	58.1	419.8	37.02	0.257	0.277	−4.1	0.188	187.3
C_5	72.2	464.8	33.35	0.305	0.267	31.8	0.239	228.2
C_6	86.0	507.5	32.46	0.344	0.268	63.9	0.275	250.1
C_7–C_9	106.5	568.2	29.21	0.418	0.262	116.0	0.346	307.3
C_{10}–C_{15}	161.7	664.1	21.82	0.622	0.249	210.5	0.523	452.2
C_{16}–C_{21}	250.8	761.0	15.63	0.932	0.233	314.1	0.758	659.2
C_{22}–C_{27}	325.9	824.4	12.29	1.183	0.215	388.0	0.942	806.6
C_{28}^+	476.1	924.0	8.76	1.616	0.187	505.6	1.180	1006.9

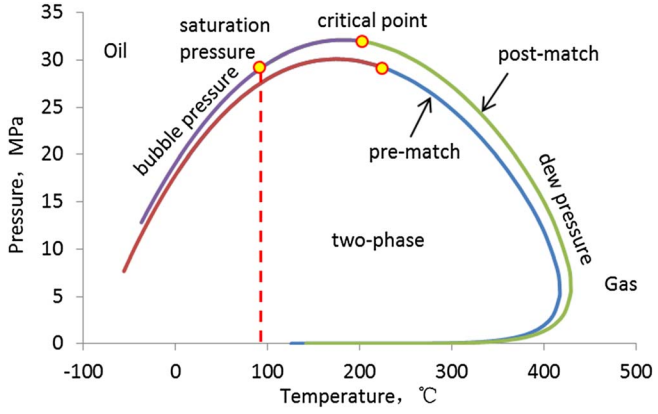

Fig. 5. P–T phase diagrams.

calculation is performed. This process simulates a condensing gas drive process, and generates the portion of the phase envelope.

4. The procedure is repeated until the liquid composition is the same as the vapor composition and MMP is the pressure at which this occurs.
5. If it is not true, then the pressure is increased to a new value and the steps 2–4 are repeated.
6. The procedure is the same for a vaporizing drive process except the third step, where the flashed vapor is mixed with the original oil at the specified gas-oil mixing ratio and then flash calculation is performed.

In our work, the gases that have been hypothesized to be injected into the reservoir are gases which are originated from the separator gas produced from this reservoir itself, as it is available from surface facilities. To further study the effect of gas compositions, removing all C_3^+ fraction of separator gas has been considered as a possible candidate. At the same time, to gain an understanding of the mechanisms of vaporizing and condensing gas drive, mixtures of CO_2 and H_2S of varying composition with CH_4 injection gas are evaluated through simulation.

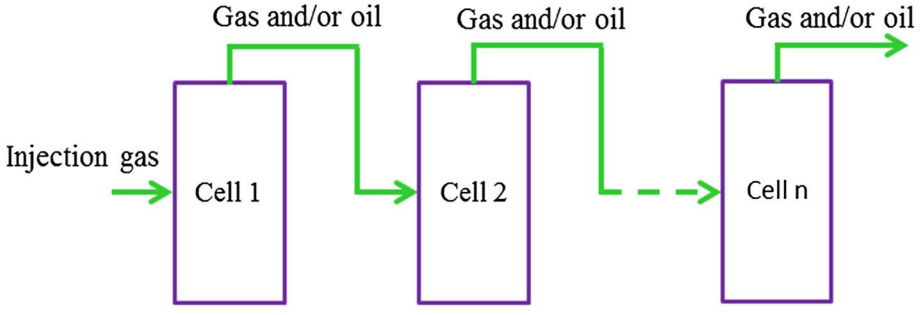

Fig. 6. Schematic diagram of cell-to-cell simulation.

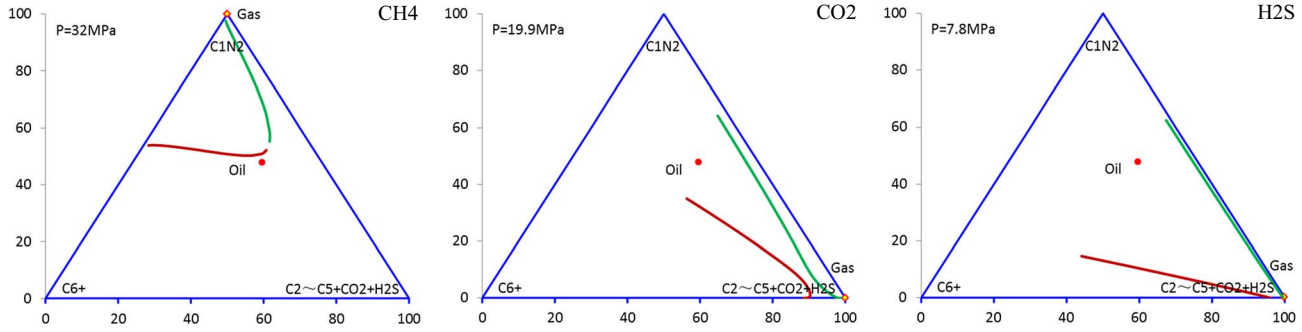

Fig. 7. Calculated pseudoternary diagrams with pure CH_4, CO_2 and H_2S injection respectively.

3.1 $CH_4/CO_2/H_2S$ solvent

3.1.1 Pure $CH_4/CO_2/H_2S$

The pseudoternary diagrams for pure CH_4, CO_2 and H_2S injection were calculated using the cell-to-cell approach. These phase envelopes are quite different when MCM was achieved. A bell-shaped phase envelope was formed for pure CH_4, a distorted hourglass shape for CO_2 and a triangle shape for H_2S shown in Figure 7. MCM of pure CO_2 injection (19.9 MPa) is lower than that of pure CH_4 injection (32 MPa), and higher than that of pure H_2S gas (7.8 MPa). The simulation results demonstrated that the sour gas containing CO_2 and H_2S achieves miscibility easier than CH_4 by the vaporization of light ended hydrocarbons. The pressure-temperature phase diagrams for these three gases were presented in Figure 8. Of course, pure H_2S injection in real oilfields is impractical because of its hypertoxicity. Simulation calculations of pure H_2S injection are only for purpose of comparison and evaluation of miscible mechanisms.

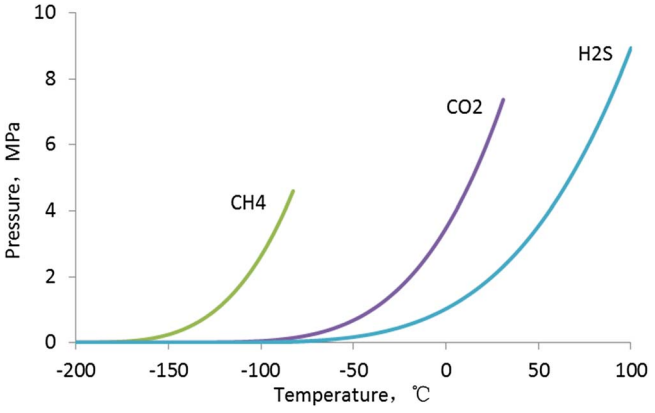

Fig. 8. P–T phase diagrams with pure CH_4, CO_2 and H_2S gases.

3.1.2 Comparison of CH_4/CO_2 and CH_4/H_2S solvent

From Figure 9, the saturation pressures of CH_4/CO_2 solvent initially increase then decrease, while the saturation pressure curve of pure CO_2 injection keeps decreasing and the curve of pure CH_4 gas increase rapidly. The maximum point of the curve is the FCM except CH_4. Calculated FCMs of CH_4/CO_2 solvents containing CH_4 being 0 mole, 0.25 mole, 0.5 mole and 0.75 mole were 29.5 MPa, 30.5 MPa, 41.2 MPa and 62.8 MPa, respectively. An increase in the amount of CO_2 in the injected gas would decrease the FCM pressures as expected. However, with CH_4 concentrations higher than a threshold value of 0.5 mole, incremental FCM pressure value would rise noticeably. These pressure-composition diagrams indicate a vaporizing process for CH_4/CO_2 solvents containing CH_4 being 0.25 mole, 0.5 mole, 0.75 mole and pure CH_4, while condensing process for pure CO_2.

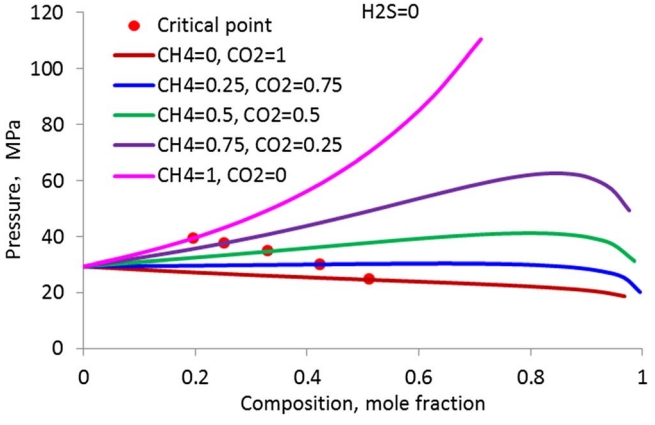

Fig. 9. Pressure-composition diagrams for CH_4/CO_2 solvent.

Multiple contact calculations were then performed with 14 components for CH_4/CO_2 solvents (CO_2 equals 0.75 mole, 0.5 mole and 0.25 mole). The corresponding pseudoternary diagrams are shown in Figure 10. MCM pressures of three mixtures gases are very close. But phase envelopes of pseudoternary diagrams between CO_2 0.5 mole and 0.25 mole are opposite directions. As CO_2 concentrations increase, MCM pressures would decrease slowly. By comparison, the FCM for all injected gas compositions was achieved at higher pressures and it appears that the variation of the injected gas composition had clear effects on FCM pressures.

The trend is very similar for pressure-composition diagrams of CH_4/H_2S solvent plotted in Figure 11. Calculated FCMs of CH_4/H_2S solvents consisting of various

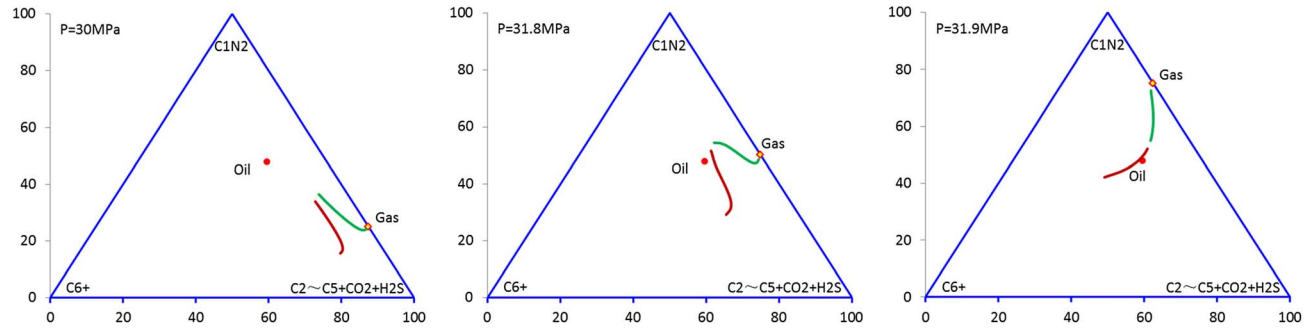

Fig. 10. Calculated pseudoternary diagrams with CH_4/CO_2 solvent (CO_2 = 0.75, 0.5, 0.25 mole).

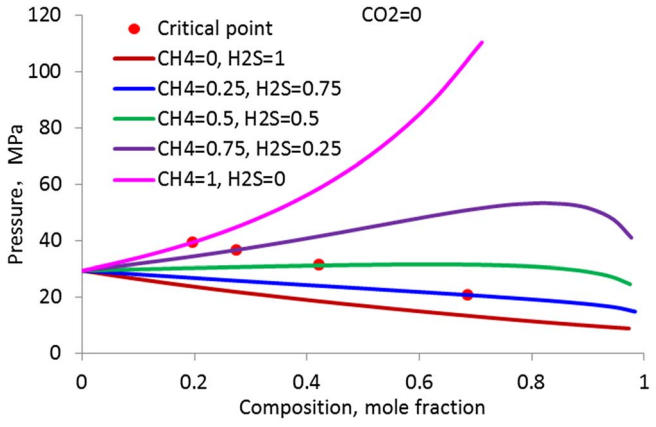

Fig. 11. Pressure-composition diagrams for CH_4/H_2S solvent.

proportions of CH_4 being 0, 0.25, 0.5 and 0.75 mole were 29.5 MPa, 29.5 MPa, 31.8 MPa and 53.7 MPa respectively. The shape of phase envelopes of pseudoternary diagrams for CH_4/H_2S are different from CH_4/CO_2, especially the CH_4/H_2S (H_2S 0.75 mole) solvent appears triangle shape similar to pure H_2S (Fig. 12).

3.1.3 $CH_4/CO_2/H_2S$ solvent

When the CH_4 concentration equals 0 mole, pressure-composition diagrams for different mole fractions of CO_2 and H_2S have a decreasing trend showed in Figure 13. As the amount of CO_2/H_2S solvent injected increases, the saturation pressure is reducing. The increase of H_2S concentrations in the injected gas decreases the MCM pressures for the reservoir oil by 0.1205 MPa/mol% (Fig. 14). FCM pressures of all mixtures are 29.5 MPa. When the CH_4 mole fraction raised to 0.25 mole, pressure-composition diagrams for different mole fractions of CO_2 and H_2S change from CO_2 0.75 mole to 0 mole plotted in Figure 15. As CO_2 concentration increases, the decreasing amplitude becomes flattened then decreases rapidly. An increase in the amount of H_2S in the injected gas would decrease MCM pressures as expected. FCM pressures would level off and attain a constant value of 29.5 MPa when H_2S concentration is higher than a threshold value of 0.15 mole (Fig. 16). When the CH_4 concentration equals 0.5 mole, pressure-composition diagrams for different mole fractions of CO_2 and H_2S vary noticeably. These shapes of pressure curves are typically increasing then decreasing and the maximum point appears (Fig. 17). Simulation results demonstrated that MCM pressures decrease relatively small, while FCM pressures decrease with H_2S increase (Fig. 18). The trend for 0.5 mole of CH_4 is very similar to 0.75 mole of CH_4. But the maximum points become larger (Fig. 19). MCM pressures of all mixtures equal 31.9 MPa and FCM pressures decrease with H_2S increase (Fig. 20).

3.2 Comparison of produced gas and deprived of its C_3^+

The main difference between produced gas and deprived of its C_3^+ is the light component content, which the

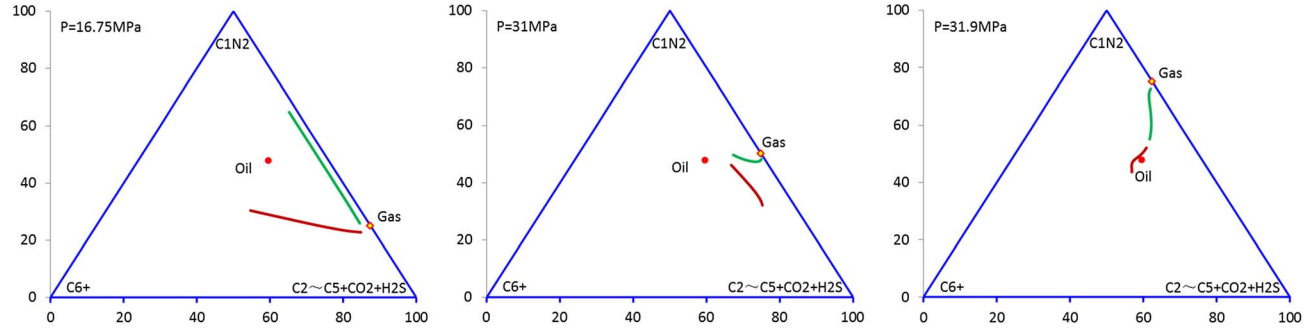

Fig. 12. Calculated pseudoternary diagrams with CH_4/H_2S solvent (H_2S = 0.75, 0.5, 0.25 mole).

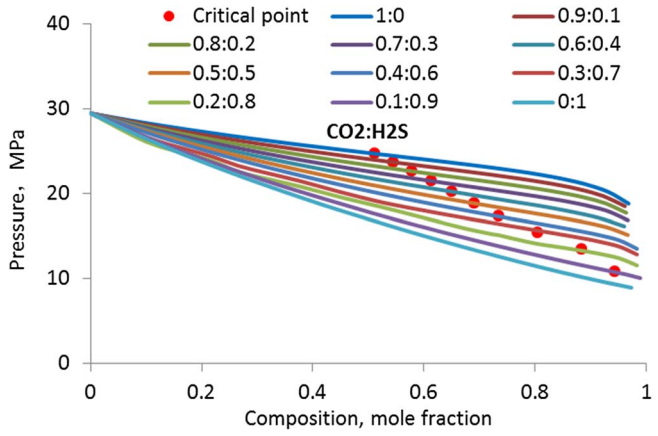

Fig. 13. Pressure-composition diagrams for different mole fractions of CO_2 and H_2S with $CH_4 = 0$ mole.

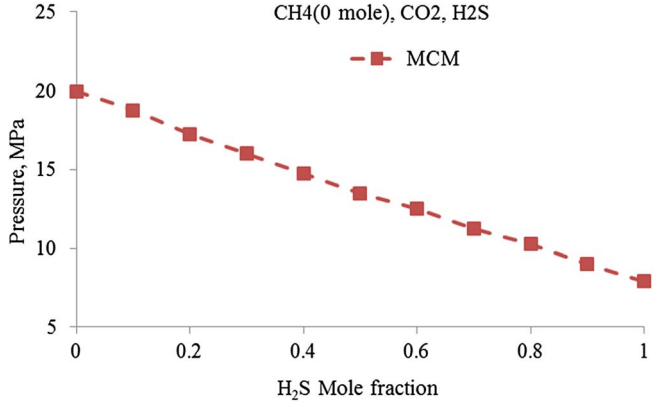

Fig. 14. MCM pressures for different mole fractions of CO_2 and H_2S with $CH_4 = 0$ mole.

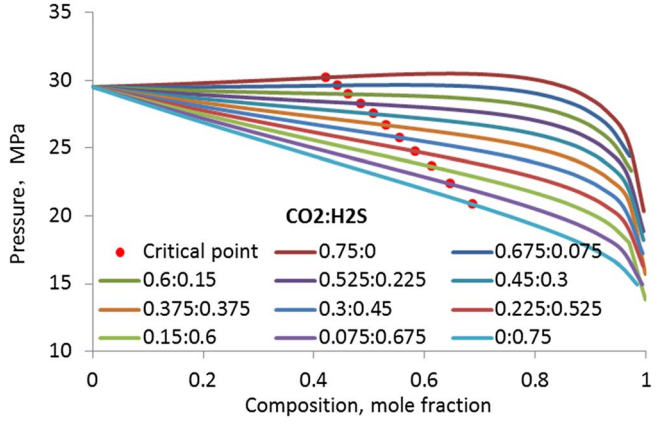

Fig. 15. Pressure-composition diagrams for different mole fractions of CO_2 and H_2S with $CH_4 = 0.25$ mole.

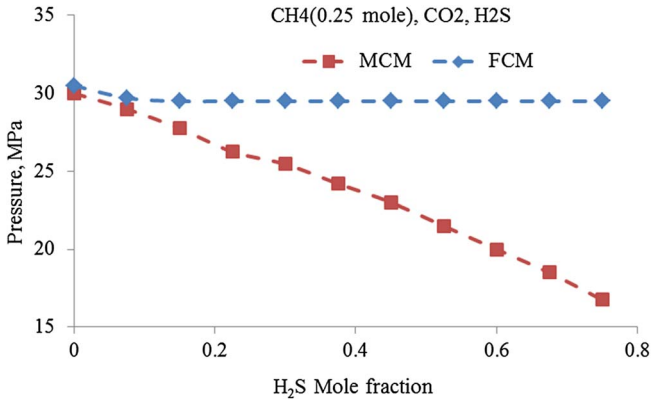

Fig. 16. MCM and FCM pressures for different mole fractions of CO_2 and H_2S with $CH_4 = 0.25$ mole.

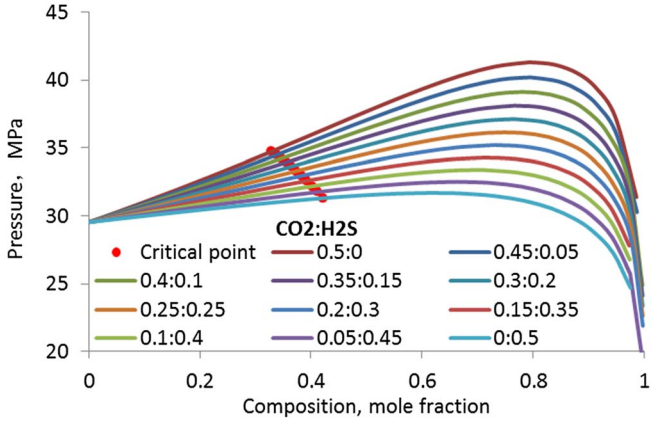

Fig. 17. Pressure-composition diagrams for different mole fractions of CO_2 and H_2S with $CH_4 = 0.5$ mole.

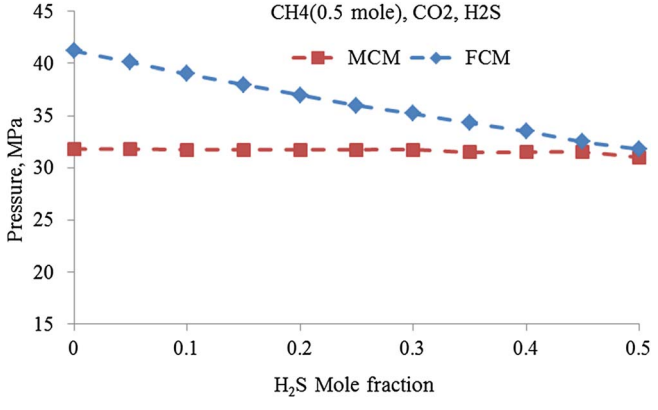

Fig. 18. MCM and FCM pressures for different mole fractions of CO_2 and H_2S with $CH_4 = 0.5$ mole.

concentrations of light components of the latter is higher than the former (Tab. 1). The pressure-composition diagram of a reservoir oil/injection gas system is a valuable tool to help identity the process mechanisms. Simulation results of pressure-composition diagrams for two types of injection gas are plotted in Figure 21. Plots indicate a

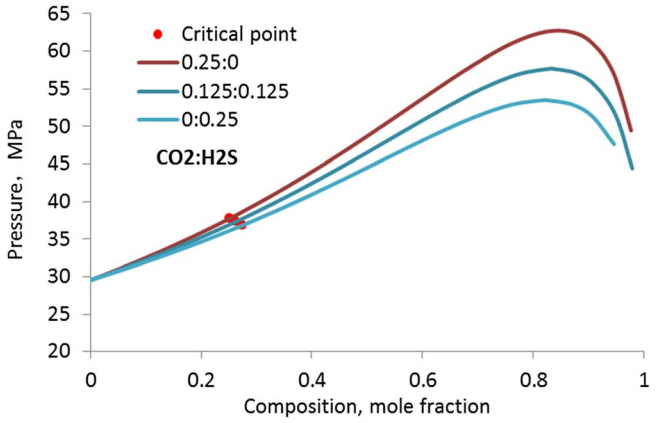

Fig. 19. Pressure-composition diagrams for different mole fractions of CO_2 and H_2S with $CH_4 = 0.75$ mole.

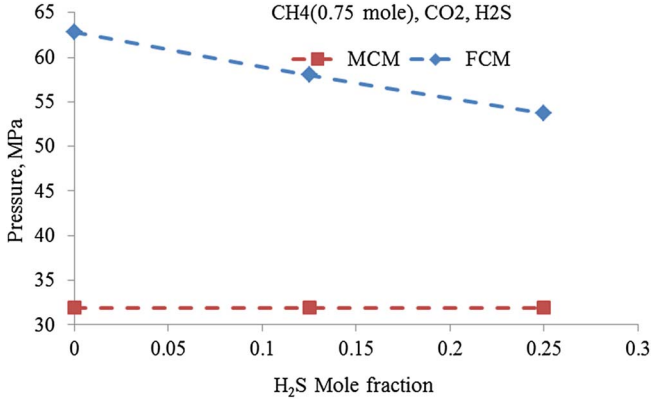

Fig. 20. MCM and FCM pressures for different mole fractions of CO_2 and H_2S with $CH_4 = 0.75$ mole.

vaporizing process rather than a condensing process since the critical point is to the left of the cricondenbar. The process is first contact miscible at 47 MPa and 52 MPa for

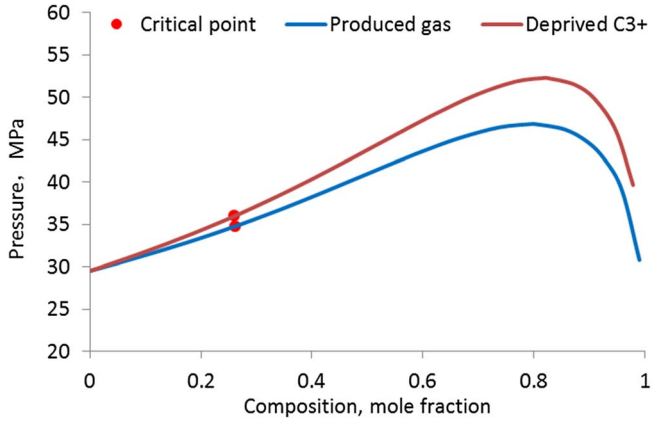

Fig. 21. Calculated pressure-composition diagrams for two types of injection gas.

produced gas and deprived C_3^+ gas respectively. It is also clear that the saturation pressure curve of the deprived C_3^+ gas is higher than produced gas. The multiple contact pseudoternary diagrams for these two types of injection gas/reservoir oil systems were calculated at several pressures (Figs. 22 and 24). The left figure in Figure 22 for produced gas/reservoir oil system indicates a vaporizing process at 30 MPa because the envelope for this process is not closed and forms an hourglass shape. Therefore miscibility was not achieved. As pressure is increased, the right figure in Figure 22 shows the diagram at 32 MPa. In this case, the phase envelope closes indicating a multiple contact miscible with the oil and the process becomes essentially a vaporizing process. Miscibility is generated by backward contacts of the equilibrium liquid phase with fresh gas (Fig. 23). So the MCM is 32 MPa.

However, from Figure 24, pseudoternary diagrams for reservoir oil/deprived C_3^+ gas system is obviously different from reservoir oil/produced gas system. The 20.25 MPa of MCM for deprived C_3^+ gas is lower than produced gas.

Due to the volatile nature of the sample oil, the full miscibility would achieve at the reservoir pressure of 77.7 MPa.

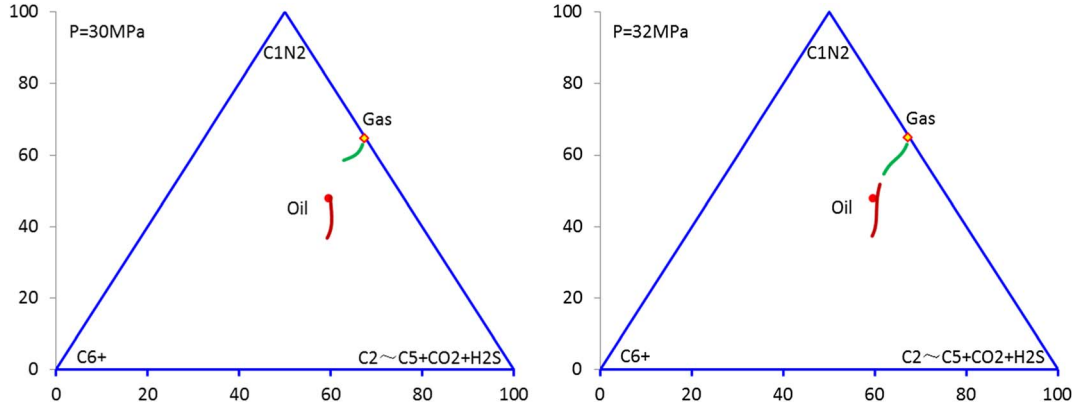

Fig. 22. Pseudoternary diagrams from multiple contact calculations for reservoir oil/produced gas system at 98 °C.

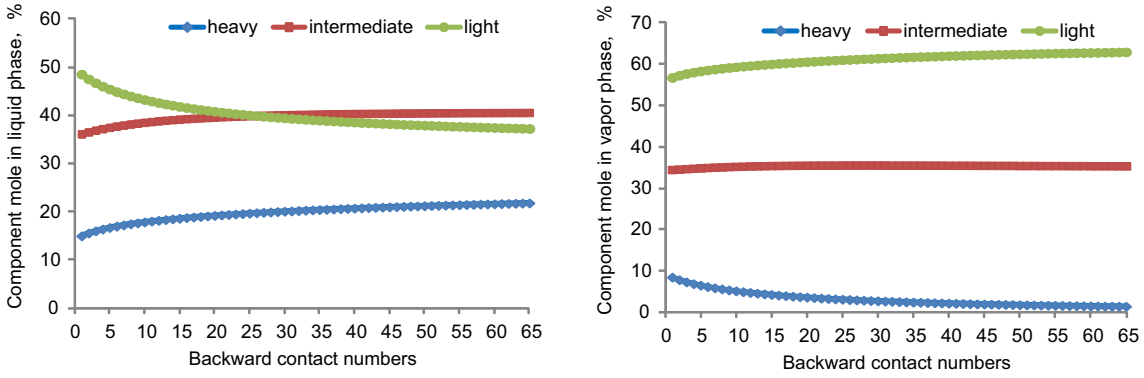

Fig. 23. Backward contact of produced gas.

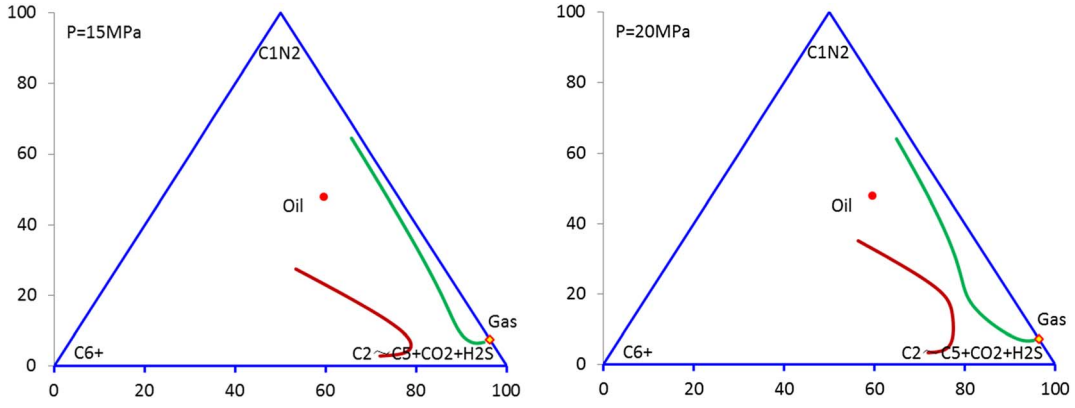

Fig. 24. Pseudoternary diagrams from multiple contact calculations for reservoir oil/deprived C_3^+ gas system at 98 °C.

4 Conclusion

A 14-component compositional simulation model was built after matching laboratory PVT data. The pressures of FCM and MCM could decrease favorably as the CO_2 and/or H_2S concentration increased in the injected stream. The envelope shape of pseudoternary diagrams relies on the composition of the injected gas. The following conclusions can be made from the previous results.

The mechanism of recovery can be identified using pressure-composition diagrams and pseudoternary diagrams generated with cubic EoS which have been tuned to match experimental data. Calculated pressures of FCM and MCM are feasible using the cell-to-cell method.

Different injection gases of $CH_4/CO_2/H_2S$ have characteristic shapes of the envelope of pseudoternary diagrams: bell shape, hourglass shape and triangle shape. This is very useful in identifying miscible mechanisms.

The volatile oil showed a nearly linear MCM pressures with mole fraction for each gas component mixed with $CH_4/CO_2/H_2S$. CO_2 and H_2S can reduce the pressure of FCM and MCM. As the CH_4 mole fraction increases, MCM pressures of mixtures would increase. FCM pressures are higher than MCM pressures. Moreover, as the CH_4 concentrations increase, the incremental FCM pressures are bigger.

Acknowledgments. The authors greatly acknowledge the financial support from the Important National Science and Technology Specific Projects of China (Grant No. 2017ZX05030-002).

References

Abrishami Y., Hatamian H. (1996) *Phase behaviour of fluids in multiple contact processes with CO_2, N_2 and their mixture.* SPE-36295.

Agarwal R.K., Li Y.K., Nghlem L. (1990) A regression technique with dynamic parameter selection for phase-behavior matching, *SPE Reserv. Eng.* **5**, 01, 115–120.

Al-Hadhrami A.K., Davis D.W., Deinum G., Soek H. (December 2007) The design of the first miscible sour gasflood project in Oman, *International Petroleum Technology Conference*, Dubai, U. A. E., 4–6 December 2007. Document ID: IPTC-11396.

Belhaj H., Abukhalifeh H., Javid K. (2013) Miscible oil recovery utilizing N_2 and/or HC gases in CO_2 injection, *J. Pet. Sci. Eng.* **111**, 144–152.

Gardner J.W., Orr F.M., Patel P.D. (1981) The effect of phase behavior on CO_2-flood displacement efficiency, *J. Pet. Technol.* 2067–2081.

Johns R.T., Ahmadi K., Zhou D., Yan M. (2010) A practical method for minimum miscibility pressure estimation of contaminated CO_2 mixtures, *SPE Reserv. Eval. Eng.* **13**, 764–772.

Johns R.T., Yuan H., Dindoruk B. (2002) *Quantification of displacement mechanisms in multicomponent gasfloods*. SPE-77696.

Luo E.H., Hu Y.L., Li B.Z., Zhu W.P. (2013a) Practices of CO_2 EOR in China, *Special Oil Gas Reserv.* **20**, 2, 1–7. (in Chinese).

Luo E.H., Hu Y.L., Li B.Z., Wang J.L., Wang Z.B. (2013b) Methods of improving sweep volume by mobility control of CO_2 flood in foreign countries, *Oilfield Chem.* **30**, 4, 613–619. (in Chinese).

Luo E.H., Zhao L., Fan Z.F., Wang J.J. (2018) *A study of PVT physical properties characteristic and compositional numerical simulation for sour gas injection*. In review.

Metcalfe R.S., Fussell D.D., Shelton J.L. (1973) A multicell equilibrium separation model for the study of multiple contact miscibility in rich-gas drives, *SPE J.* **13**, 03, 147–155.

Nutakki R., Hamoodi A.N., Li Y.-K., Nghiem L.X. (1991) *Experimental analysis, modelling, and interpretation of recovery mechanisms in enriched-gas processes*. SPE-22634.

Pederson K.S., Fjellerup J., Thomassen P., Fredenslund A. (1986) *Studies of gas injection into oil reservoirs by a cell-to-cell simulation model*. SPE-15599.

Stalkup F.I. (1987) *Displacement behavior of the condensing/vaporizing gas drive process*. SPE-16715.

Tang Y., Sun L., Zhou Y.Y., Li S.L., Sun L.T., Du Z.M. (2005) Mechanism evluation of condensing/vaporizing miscible flooding with hydrocarbon-rich gas injection, *Pet. Explor. Dev.* **32**, 2, 133–136.

Urazgaliyeva G., King G.R., Darmentaev S., Tursinbayeva D., Dunger D., Howery R., Zalan T., Lindsell K., Iskakov E., Turymova A., Jenkins S., Walker C., Bateman P., Aitzhanov A. (2014) Tengiz sour gas injection project: An update, *SPE Annual Caspian Technical and Exhibition*, Astana, Kazakhstan, 12–14 Bivermber 2014. Document ID: SPE-172284.

Wang S., Yeskaiyr B., Walker C. (October 2014) A sector model for IOR/EOR process evaluation, *SPE Annual Technical Conference and Exhibition*, Amsterdam, The Netherlands, 27–29 October 2014. Document ID: SPE-170605.

Zhang C.S., Fan Z.F., Xu A.Z., Zhao L., Zhao L.D., Luo E.H. (2017) Study on miscible mechanism of recycle dissolved gas in volatile oil reservoir with acid gas, *Reserv. Eval. Dev.* **7**, 2, 41–46.

Zick A.A. (1986) *A combined condensing/vaporizing mechanism in the displacement of oil by enriched gases*. SPE-15493.